JOURNAL OF SOLID STATE CHEMISTRY 97, 434–442 (1992)

Metal–Semiconductor Transition in Oxygen-Deficient Layered Perovskite Compounds of $Sr_4V_3O_{10-\delta}$

NAOKI OHASHI, YOSHINOBU TERAMOTO,* HIROYUKI IKAWA, AND OSAMU FUKUNAGA

Department of Inorganic Material, Tokyo Institute of Technology, 2-12-1O-Okayama, Meguro-ku, Tokyo 152, Japan

AND JUNZO TANAKA

National Institute for Research in Inorganic Materials, 1-1 Namiki, Tsukuba-shi, Ibaraki 305, Japan

Received August 19, 1991

$Sr_4V_3O_{10-\delta}$ was prepared by solid state reaction with controlling oxygen deficiency (δ). When the δ-value increased, carrier concentration decreased and electrical conduction changed from metallic to semiconducting while, simultaneously, the effective magnetic moment increased and the magnetic property changed from Pauli paramagnetism to normal paramagnetism. The temperature dependence of resistivity below 20 K was described by $\rho = A \exp(-B/T^{1/4})$. The X-ray photoelectron spectra of V_{2p} consisted of two peaks which were related to V^{3+} and V^{4+} ions. These results suggest that the metal–semiconductor transition in $Sr_4V_3O_{10-\delta}$ is due to a randomness of potential caused by trivalent vanadium ions and oxygen deficiencies. © 1992 Academic Press, Inc.

I. Introduction

Since the discovery of a cuprate superconductor (*1*), much research on its related compounds has been performed (*2*). Their crystallostructural feature is alternative stacking of a two-dimensional conduction layer and a blocking layer, for example, a CuO_6 perovskite layer and a (La,Sr)–O rock salt layer in $(La_{1-x},Sr_x)_2CuO_4$ (*3*).

Another feature of the cuprate superconductors is that superconductivity appears in a transient region between the insulator and normal metal (*4, 5*). Further, it is known that their superconducting transition temperatures (T_c) increase with both carrier concentrations (*6, 7*) and the number of Cu–O layers per unit cell (*8, 9*).

These features of the cuprate superconductors seem to be a plausible guideline applicable to synthesis of a new high T_c superconductor with or without copper.

Cyrot *et al.* (*10*) synthesized a K_2NiF_4-type vanadate of $Sr_2VO_{4-\delta}$. They reported that $Sr_2VO_{4-\delta}$ was an antiferromagnetic insulator (*10*). On the other hand, its related compounds such as $Sr_3V_2O_7$ (*11*) and $Sr_4V_3O_{10}$ (*12*) also have been reported to be layered perovskite compounds with alternative stacking of VO_6 perovskite-type layers and SrO rock-salt-type layers. Because of the structural similarity, $Sr_4V_3O_{10-\delta}$,

* Present address: Mitsubishi Trust and Banking Co., Ltd. 2-19-12 Shibuya, Shibuya-ku, Tokyo 150, Japan.

0022-4596/92 $3.00

Copyright © 1992 by Academic Press, Inc.
All rights of reproduction in any form reserved.

$Sr_3V_2O_{7-\delta}$, $Sr_2VO_4{}^{-\delta}$, and/or their related compounds are expected to satisfy the above-mentioned conditions for superconductivity.

In the present study, $Sr_4V_30_{10-\delta}$ with three perovskite layers was prepared by controlling oxygen deficiencies (δ). The crystal structure was refined by a Reitvelt method in III-1. The Hall effect and magnetic susceptibility were measured to elucidate their electrical (III-2) and magnetic properties (III-3). X-ray photoelectron spectra were measured to obtain the effect of oxygen deficiency on the electronic structure of $Sr_4V_3O_{10-\delta}$ (III-4).

II. Experimental Procedures

II-1. Sample Preparation

$Sr_4V_3O_{10-\delta}$ was prepared by three steps in the first step, a mixture of $SrCO_3$ (G.R. grade) and V_2O_5 (99.9% in purity) with an atomic ratio of Sr/V = 4/3 was fired in air at 1000°C for 12 hr. In this stage, the product was a mixture of two major phases, $Sr_3V_2O_8$ and $Sr_2V_2O_7$, which were identified by the powder X-ray diffraction technique.

In the second step, the product was milled, pelletized, and reduced in 1 bar of H_2 gas at 1100°C for 24 hr. After this reduction process, the sample became an almost single phase of $Sr_4V_3O_{10-\delta}$ with a trace of $Sr_3V_2O_8$.

Finally, the reduced pellets were milled, pelletized again, and sintered under 1 bar of H_2 gas at 1400°C for 24 hr. In this stage, the sintered pellets became a single phase of $Sr_4V_3O_{10-\delta}$.

The sintered pellets were annealed under 1 bar of H_2 gas at temperatures between 600 and 1000°C for 50 hr to control the amount of oxygen deficiency (δ). Hereafter, the samples sintered at 1400°C and annealed at 1000, 800, and 600°C are abbreviated as AN1400, AN1000, AN800, and AN600, respectively.

II-2. Characterization of the Samples

The amount of oxygen deficiency was determined from a weight gain after the following oxidation process. The oxidation was repeatedly performed at 800°C in a stream of 1 bar of O_2 gas until the weight of the sample was stable within 0.01% of the initial weight. The valence of vanadium ion after the oxidation was supposed to be +5 to calculate δ and the average valence of vanadium ions.

Lattice constants of $Sr_4V_3O_{10-\delta}$ at room-temperature were determined by X-ray powder diffraction with a least-squares method. The diffraction angles were calibrated by an internal standard of Si powder (99.99% in purity).

The crystal structure of AN1400 was refined by a Rietvelt method (RIETAN program (*13*)) for an X-ray powder diffraction profile based on the structure parameters of $Sr_4Ti_3O_{10-\delta}$ (*14*). The number of intensity data was 5001, all of which were collected in a region of $20° < 2\theta$ (Cu$K\alpha$) $<120°$.

Electric resistivity (ρ) was measured by an ordinary dc four-probe method in a temperature range between room temperature and 6 K. Hall coefficients R_H were measured by a Van der Pauw method (*15*) with a Resitest 8200 system (Toyo Co.). The samples were 7 × 7 × 0.4 mm^3 in size. In the measurements, the applied field was H = 10 kOe and the loaded current was I = 20–100 mA. The temperature range was between 300 and 90 K for AN1400 and AN800.

The magnetic susceptibility of $Sr_4V_3O_{10-\delta}$ was measured with a SQUID magnetometer (Quantum Design Co., Ltd.) by a field cooling method in a temperature range between 300 and 5 K under a magnetic field of 10 kOe.

X-ray photoelectron spectra were taken with a Microlab 320D associated with an X-ray source of Al$K\alpha$ radiation (V.G. Scientific, Ltd.). Samples were entered into an

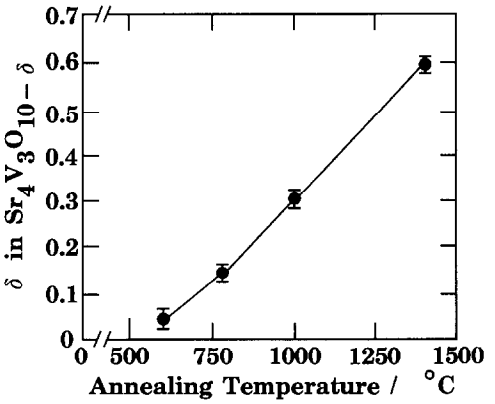

FIG. 1. Annealing temperature dependence of oxygen deficiency δ in $Sr_4V_3O_{10-\delta}$.

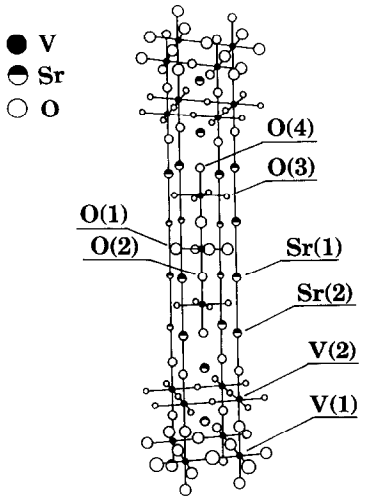

FIG. 3. Crystal structure of AN1400 refined by the Rietvelt method. This figure was drawn by the ORTEP program (*20*). Radii of the spheres are proportional to isostatic thermal parameters.

ultrahigh vacuum chamber as soon as they were scraped in air. Pressure in the chamber during measurement was less than 3.5×10^{-9} mbar.

III. Experimental Results and Discussion

III-1. Crystal Structure and Oxygen Deficiencies

The amount of oxygen deficiency (δ) is shown as a function of annealing temperature in Fig. 1. The maximal δ-value was observed for AN1400: $\delta = 0.59$. The δ-value of $Sr_4V_3O_{10-\delta}$ decreased with the decrease in annealing temperature and became very small in AN600 ($\delta = 0.03$).

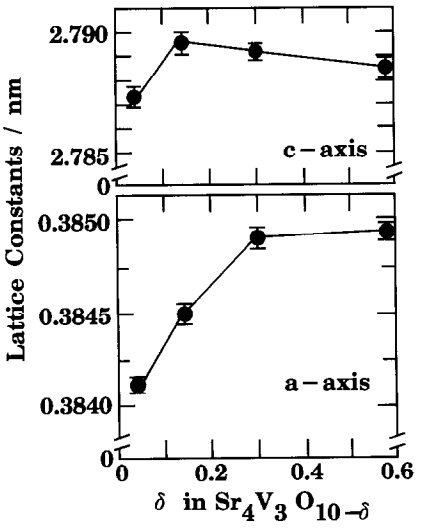

FIG. 2. Oxygen deficiency δ dependence of lattice constants of $Sr_4V_3O_{10-\delta}$.

Figure 2 shows the δ-dependence of lattice constants measured at room temperature. Lattice constants in a higher δ-value region are almost independent of the δ-value. This behavior is similar to that observed in a perovskite-type vanadate of $SrVO_{3-\delta}$ (*16*) and therefore implies that the oxygen deficiencies in $Sr_4V_3O_{10-\delta}$ are located in the perovskite-like layers.

The result of Rietvelt analysis is shown in Fig. 3 and Table I. As shown in Table I, isostatic thermal parameters of O(1) and O(2) in AN1400 are larger than that of the other oxygen sites. This result suggests a possibility that the oxygen deficiencies locate at O(1) and O(2) sites.

III-2. Electrical Properties

The temperature dependence of electric resistivity of $Sr_4V_3O_{10-\delta}$ is shown in Fig.

TABLE I

STRUCTURAL PARAMETERS OF AN1400 REFINED BY THE RIETVELT METHOD

Composition				$Sr_4V_3O_{9.41}$	
Symmetry				Tetragonal	(*P4/mmm*)
Lattice constants (nm)				a = 0.3843,	c = 2.789
Atom	Site	x	y	z	B_{iso}[a] (nm^2)
Sr(1)	4*e*	0	0	0.431	0.004
Sr(2)	4*e*	0	0	0.298	0.005
V(1)	2*a*	0	0	0	0.003
V(2)	4*e*	0	0	0.139	0.003
O(1)	4*c*	0	½	0	0.01
O(2)	4*e*	0	0	0.07	0.01
O(3)	8*g*	0	½	0.14	0.003
O(4)	4*e*	0	0	0.21	0.007

Reliability factors

R_{WP}	R_P	R_I	R_F	R_E
0.099	0.073	0.022	0.017	0.035

Note. The occupation factor of each site was fixed to 1.00.
[a] Isostatic thermal parameter.

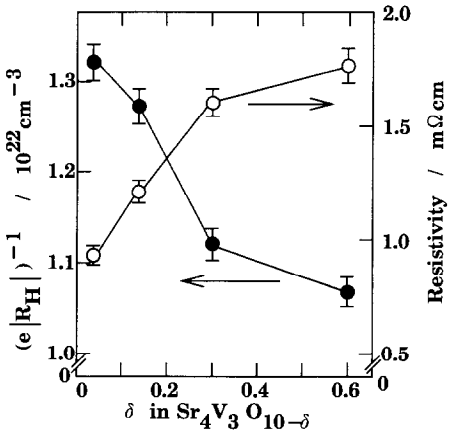

FIG. 5. Oxygen deficiency δ dependence of carrier concentration $(e|R_H|)^{-1}$ (closed circle) and electric resistivity (open circle) of $Sr_4V_3O_{10-\delta}$ at room temperature.

4. Neither a superconducting transition nor any anomaly of resistivity was observed in the present study. However, the metal–semiconductor transition occurred between δ = 0.30 (AN1000) and δ = 0.14 (AN800).

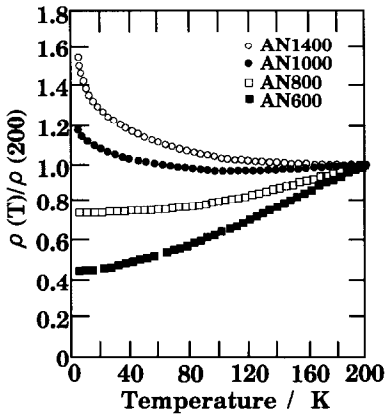

FIG. 4. Temperature dependence of electric resistivity of $Sr_4V_3O_{10-\delta}$. Resistivity was normalized by the value at 200 K. Open circle, AN1400; closed circle, AN1000; open square, AN800; and closed square, AN600.

Hall coefficients R_H of the present samples are all negative, which means that the carrier is an electron. The values of $(e|R_H|)^{-1}$ at room temperature together with electrical resistivities at room temperature as a function of δ are shown in Fig. 5. Supposing the single carrier approximation, $(e|R_H|)^{-1}$ corresponds to the concentration of the effective carrier.

The value of $(e|R_H|)^{-1}$ of $Sr_4V_3O_{10-\delta}$ decreases with the increase in the δ-value. In general, it is considered that oxygen deficiencies in *n*-type oxide semiconductors are donors as observed in $BaTiO_3$, $SrTiO_3$, etc. (*17*); nevertheless, $(e|R_H|)^{-1}$ of $Sr_4V_3O_{10-\delta}$ decreases with the increase of the δ-value. The effect of oxygen deficiency in $Sr_4V_3O_{10-\delta}$ on the electrical properties is different from that in perovskite titanate compounds, suggesting that the electrons in the conduction band, which is thought to be mainly formed from the V_{3d} orbital, are localized by the introduction of oxygen deficiencies.

Temperature dependencies of carrier concentration $(e|R_H|)^{-1}$ and mobility $|R_H|/\rho$ of AN1400 and AN800 are shown in Fig. 6.

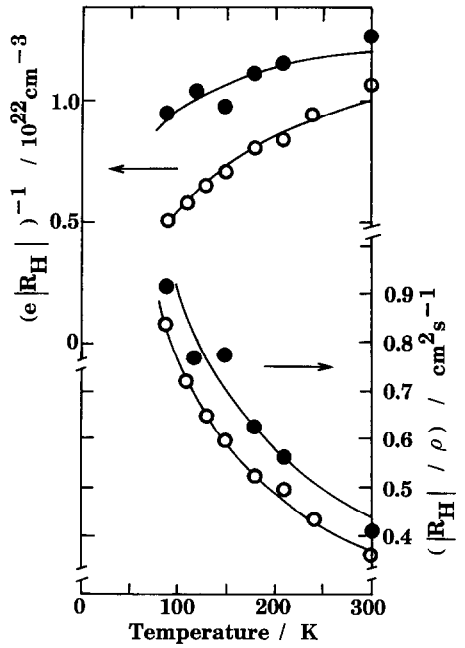

FIG. 6. Temperature dependence of carrier concentration $(e|R_H|)^{-1}$ and mobility R_H/ρ of AN1400 and AN800. Open and closed circles indicate AN1400 and AN800, respectively.

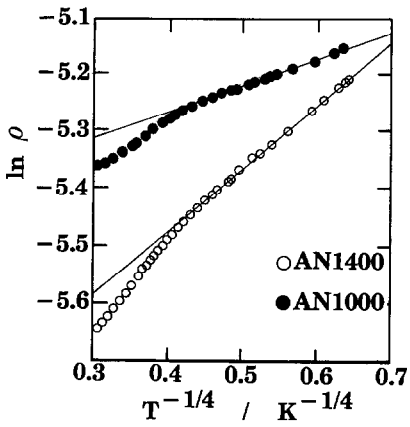

FIG. 7. Electric resistivity against $T^{(-1/4)}$. Solid line shows the best fit of temperature dependence of resistivity to $\rho = \rho_0 \exp(-B/T^{(1/4)})$.

This figure suggests that the carriers are of a thermal activation type.

The carrier concentration n_H and mobility μ_H are fitted by the following equations, respectively:

$$(e|R_H|)^{-1} = n_H = n_0 \exp[-(\Delta E/T)] \quad (1)$$

$$|R_H|/\rho = \mu_H = AT^{-\alpha}. \quad (2)$$

Solid lines in Fig. 6 show the best fits of Eqs. (1) and (2). Fitting parameters of n_0, ΔE, A, and α are listed in Table II. As seen in Table II, preexponential factors n_0 are independent of the δ-value. This result indicates that the oxygen deficiencies affect neither the density of state of the Fermi level nor the donor concentration; however, the activation energies and mobilities are affected by them.

TABLE II

PARAMETERS DETERMINED BY A FITTING OF $(e|R_H|)^{-1}$ AND $|R_H|/\rho$ TO EQS. (1) AND (2) IN THE TEXT, RESPECTIVELY

Sample	δ	n_0 (10^{22}cm^{-3})	ΔE (K)	A	α
AN1400	0.59	1.38	92	16	0.66
AN800	0.14	1.39	35	19	0.66

Below 90 K, the resistivity of AN1400 was lower than the value calculated by the parameters in Table II and Eq. (3),

$$\rho(t) = 1/(en_H\mu_H). \quad (3)$$

This deviation suggests that the conduction mechanism of the carrier is different below and above 90 K.

Mott and Davis (*18*) proposed variable range hopping for the electrical conduction in a random system. In the variable range hopping model, the resistivity was described by Eq. (4),

$$\rho = A \exp[-B/T^{(1/4)}]. \quad (4)$$

By plotting ln ρ versus $T^{-(1/4)}$, the resistivities of AN1400 and AN1000 lie on straight lines at low temperature ($T < 20$ K) as shown in Fig. 7. From this result, it is conjectured that the variable range hopping conduction takes place at lower temperature in the semi-

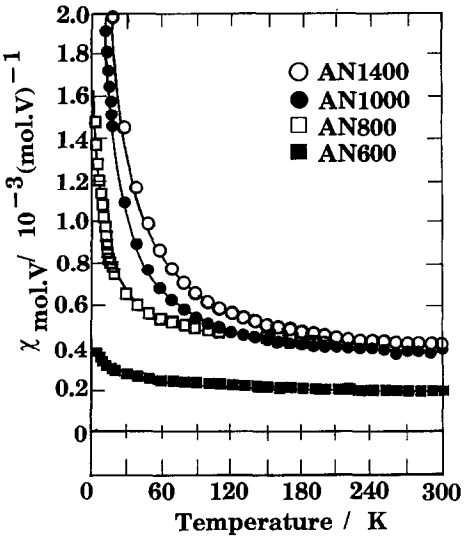

FIG. 8. Temperature dependence of magnetic susceptibility of $Sr_4V_3O_{10-\delta}$. Open circle, AN1400; closed circle, AN1000; open square, AN800; and closed square AN600.

conducting $Sr_4V_3O_{10-\delta}$. In the temperature region between $T = 20$ K and $T = 100$ K, both hopping and carrier activation may occur simultaneously. The conduction mechanism will be discussed in III-5 in relation to the electronic structure.

III-3. Magnetic Properties

Temperature dependencies of magnetic susceptibility χ are shown in Fig. 8. The magnetic susceptibility of AN600 was changed slightly with the temperature below 60 K while it is almost independent of temperature above 60 K. The Pauli paramagnetic behavior of AN600 is consistent with its metallic conduction. However, a slight increase of magnetic moments in the χ–T curve in the lower temperature region suggested that a small part of the carrier in AN600 is localized to induce the magnetic moment.

The magnetic susceptibilities of AN800, AN1000, and AN1400 were described by the

TABLE III

MAGNETIC PARAMETERS OF $Sr_4V_3O_{10-\delta}$

Sample	d	C	θ (K)	χ_0 (mole V)$^{-1}$	μ_p/μ_B
AN1400	0.59	3.4×10^{-2}	−1.2	3.0×10^{-4}	1.03
AN1000	0.30	2.3×10^{-2}	−0.7	3.0×10^{-4}	0.85
AN800	0.14	1.0×10^{-2}	−5.2	3.8×10^{-4}	0.57

Note. C, θ, and χ_0 are determined by fitting the temperature dependence of magnetic susceptibility $\chi(T)$ to $\chi(T) = C/(T - \theta) + \chi_0$.

Curie–Weiss law and no magnetic anomaly was observed in the temperature region between 5 and 300 K. Curie constants and temperatures determined by a least-squares method are listed in Table III. Curie temperatures are almost zero for all samples, suggesting that the magnetism of the semiconducting samples is normal paramagnetic without any magnetic ordering.

Curie constants increase with the δ-value. This is opposite to the behavior of the carrier concentration which decreases with the δ-value. As listed in Table III, effective magnetic moments μ_p are smaller than those of free V^{3+} (2.83 μ_B) and V^{4+} (1.73 μ_B) ions, where μ_B is the Bohr magneton. Such small values of μ_p also suggest that some part of the carrier is itinerant and the rest is localized; the latter has the magnetic moment. This is consistent with the discussion on the Hall effect.

III-4. Photoelectron Spectroscopy

The X-ray photoelectron spectra (XPS) of the V ion in AN1400 (A) and AN600 (B) are shown in Fig. 9. Peaks observed between 510 and 520 eV are ascribed to $V_{2p}3/2$. The $V_{2p}3/2$ peak of AN600 is relatively sharp compared with that of AN1400.

The difference between the spectra of AN1400 and AN600 is also shown in Fig. 9: positive and negative peaks appear in the difference profile. This result suggests that the $V_{2p}3/2$ spectrum of AN1400 consists of two peaks. A shoulder at the lower energy

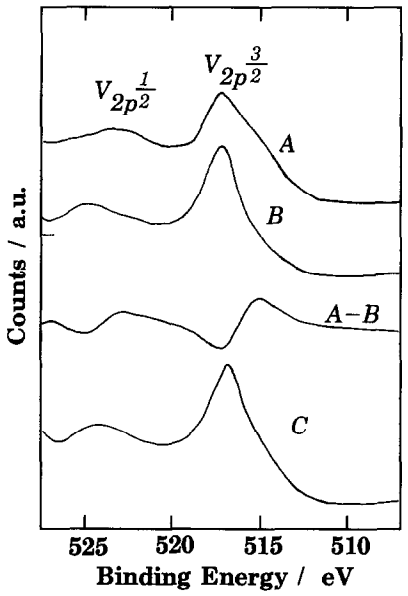

FIG. 9. X-ray photoelectron spectra of the V_{2p} core level of (A) AN1400 with $V^{3.6+}$, (B) AN600 with $V^{4.0+}$, (A − B) difference profile between XPS of AN1400 and AN600, and (C) $SrVO_{2.8}$ with $V^{3.6+}$.

side of the $V_{2p}3/2$ peak of AN1400, which corresponds to the positive peak of the difference profile, is considered to relate to V^{3+} ions. Therefore, comparing AN1400 with AN600, the amount of V^{4+} ions decreases and that of V^{3+} ions increases in AN1400.

The bottom spectrum in Fig. 9 is for $SrVO_{2.8}$ with the average valence of V (+3.6) the same as that of AN1400. However, the shape of the $V_{2p}3/2$ peak of $SrVO_{2.8}$ is rather similar to that of AN600 with V^{4+}. The different average valences between $SrVO_{2.8}$ and AN600 are seen as the different binding energies: the binding energy of AN600 is higher than that of $SrVO_{2.8}$. This result suggests that the valence state of V ions in $SrVO_{2.8}$ is averaged; that is, their V_{3d} electrons are delocalized. Conversely, these results suggest that the valence V ions are not averaged and that V^{3+} and V^{4+} ions coexist in AN1400. Taking into account that AN1400 is of the activated type while AN600 is metallic, the V_{3d} electrons of V^{4+} ions are delocalized in AN1400 and in AN600.

III-5. Electronic Structures

Dougier and Hagenmuller (*19*) reported metal–semiconductor transition in a solid solution system of $(La_{1-x},Sr_x)VO_3$ and discussed the modification of electronic structure due to the substitution of Sr. The metal–semiconductor transition occurred at $x = 0.225$, below which the semiconducting behavior appeared ($x < 0.225$). Further, the semiconducting region was classified into two cases. In a lower x region of semiconducting $(La_{1-x},Sr_x)VO_3$, the carriers were localized by a Hubbard gap and the magnetic property was antiferromagnetic, while in a higher x region of semiconducting $(La_{1-x},Sr_x)VO_3$, the carriers were localized by random potential.

Mott and Davis (*18*) studied the effect of random potential on electrical conduction. According to them, random potential induces the localization of the carrier; that is, a mobility edge is formed by it in the conduction band.

It is thought that the metal–semiconductor transition of $Sr_4V_3O_{10-\delta}$ occurs by the mechanism shown in Fig. 10. Figures 10a and 10b show band models of metallic and

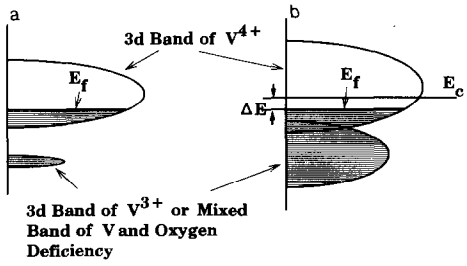

FIG. 10. Schematic figure of the conduction band of (a) metallic and (b) semiconducting $Sr_4V_3O_{10-\delta}$. E_c and E_f indicate the mobility edge and Fermi level, respectively.

semiconducting $Sr_4V_3O_{10-\delta}$ with mobility edge E_c, respectively.

Figure 10a corresponds to the metallic $Sr_4V_3O_{10-\delta}$ AN600. The amount of the V^{3+} ion is considerably smaller than that of the V^{4+} ion and therefore the effect of the V^{3+} ion and/or oxygen deficiency is minor. The mobility edge is thought not to be formed in the conduction band as shown in Fig. 10a or to be formed below Fermi level E_f. Metallic conduction of AN600 is consistent with the model of Fig. 10a. The Pauli paramagnetic behavior in the high temperature region and normal paramagnetic behavior in the low temperature region of AN600 as shown in Fig. 8 are ascribed to the itinerant electrons of V^{4+} ions and the localized electrons of V^{3+} ions, respectively.

Figure 10b represents the band scheme of the semiconducting $Sr_4V_3O_{10-\delta}$ AN1000 and AN1400. The small μ_p and the semiconducting behavior can be explained by the formation of the mobility edge in the conduction band. The result of XPS of AN1400 suggests an increase of the fraction of the localized V_{3d} electron related to the V^{3+} ion. The band of V^{3+} ions and/or oxygen deficiencies is formed below the band of V^{4+} ions and they possibly overlap each other. As the oxygen deficiency and V^{3+} and V^{4+} ions are considered to be randomly distributed, the random potential due to them can produce the mobility edge. In the case of the activation energy, ΔE in Eq. (1) is therefore related to the energy difference between the Fermi level and the mobility edge: $E_f - E_c$. The increase of Curie constants in Table III is considered to be related to the increase of the amount of V^{3+} ions whose electrons are localized below the mobility edge and have the magnetic moment.

V. Conclusion

The oxygen-deficient layered perovskite compound of $Sr_4V_3O_{10-\delta}$ was prepared by controlling the amount of oxygen deficiencies by annealing at various temperatures. The electric resistivity of $Sr_4V_3O_{10-\delta}$ was increased with the increase of the amount of oxygen deficiencies and metal–semiconductor transition was observed between $\delta = 0.14$ and $\delta = 0.30$. The localization of the carrier could be explained by the mobility edge formed by the random potential of V^{3+} ions and/or oxygen deficiencies.

Neither superconducting transition nor antiferromagnetic transition in $Sr_4V_3O_{10-\delta}$ was observed in the present study. If the antiferromagnetic ordering is essential for high T_c superconductivity to appear, $Sr_4V_3O_{10-\delta}$ does not satisfy the condition for a high T_c superconductor. However, as the perovskite-type titanate of $SrTiO_3$ (*17*) is a low T_c superconductor without antiferromagnetic ordering, the possibility of superconductivity in $Sr_4V_3O_{10-\delta}$ still might be expected.

Acknowledgments

The authors thank Dr. M. Umehara of NIRIM for useful discussions. The authors give thanks to M. Takemoto, T. Komiya, and H. Iwama of T.I.T. for their kind help in sample preparation and to Mr. T. Akita of Taiyo Yuden Co., Ltd., for his kind help in XPS measurements. This study was partly supported by a Grant-in-Aid for Scientific Research on "Chemistry of the Superconductor" from the Ministry of Education, Science, and Culture in Japan.

References

1. J. G. Bednorz and K. A. Muller, *Z. Phys. B* **64,** 1989 (1986).
2. N. Ohashi, H. Ikawa, O. Fukunaga, and J. Tanaka, *Physica C* **166,** 465 (1989).
3. S. Uchida, H. Takagi, K. Kitazawa, and S. Tanaka, *Jpn. J. Appl. Phys.* **26,** L1 (1987).
4. H. Takagi, T. Ido, S. Ishibashi, M. Uota, and S. Uchida, *Phys. Rev. B* **40,** 2254 (1989).
5. H. Takagi, S. Uchida, and Y. Tokura, *Phys. Rev. B* **62,** 1197 (1989).
6. Q. Zhengnan, B. Okai, J. Tanaka, H. Nozaki, M. Ohta, and M. Matsunaga, *Jpn. J. Appl. Phys.* **28,** L1131 (1989).
7. N. Ohashi, H. Ikawa, O. Fukunaga, M. Kobayashi, and J. Tanaka, *Physica C* **177,** 377 (1991).

8. J. AKIMITSU, A. YAMAZAKI, H. SAWA, AND H. FUJIKI, *Jpn. J. Appl. Phys.* **26,** L2080 (1987).
9. H. MAEADA, Y. TANAKA, M. FUKUTOMI, AND T. ASANO, *Jpn. J. Appl. Phys.* **27,** L209 (1988).
10. M. CYROT, B. LAMBERT-ANDERSON, J. L. SOUBEYROUX, M. J. RAY, PH. DAHAUT, F. CRYOT-LACKMAN, G. FOURCAUDOT, J. BEILLE, AND J. L. THOLENCE, *J. Solid State Chem.* **85,** 321 (1990).
11. T. SHINIKE, T. SAKAI, G. ADACHI, AND J. SHIOKAWA, *Mater. Res. Bull.* **11,** 801 (1976).
12. M. ITOH, M. SHIKANO, R. LIANG, H. KAWAJI, AND T. NAKAMURA, *J. Solid State Chem.* **88,** 597 (1990).
13. F. IZUMI, H. ASANO, AND N. WATANABE, *J. Appl. Crystallogr.* **20,** 411 (1987).
14. R. W. G. WYCOFF, "Crystal Structures," 2nd ed., Vol. 1, p. 443, Interscience, New York (1965).
15. L. J. VAN DER PAUW, *Philips Res. Rep.* **13,** 1 (1958).
16. M. J. KESTIGIAN, J. G. DICKINSON, AND R. WARD, *J. Am. Chem. Soc.* **79,** 5598 (1957).
17. F. S. GALASSO, "Structure, Properties and Preparation of Perovskite-Type Compounds," Chap. 4, Pergamon, Oxford (1969).
18. N. F. MOTT AND E. A. DAVIS, "Electronic Processes in Non-Crystalline Materials," 2nd ed., Oxford Univ. Press, Oxford (1979).
19. P. DOUGIER AND P. HAGENMULLER, *J. Solid State Chem.* **15,** 158 (1975).
20. C. K. JOHNSON, "ORTEP II," Report ORNL-5138, Oak Ridge National Laboratory, Oak Ridge, TN.